Polymer Chemistry

PAPER

View Article Online
View Journal | View Issue

Cite this: *Polym. Chem.*, 2016, **7**, 2253

A charge-conversional intracellular-activated polymeric prodrug for tumor therapy

Yue Wang,[a,b] Shixian Lv,[b] Mingxiao Deng,*[a] Zhaohui Tang*[b] and Xuesi Chen[b]

Received 7th October 2015,
Accepted 12th February 2016

DOI: 10.1039/c5py01618e

www.rsc.org/polymers

Stimuli-responsive drug-delivery systems have attracted great attention for controlled drug release. The pH value is relatively low in the tumor tissues and the concentration of glutathione is significantly high in the cells. According to these features, a charge-conversional polymeric prodrug that is sensitive to pH and redox is designed. 3,3′-Dithiodipropionic acid modified paclitaxel (DTPA-PTX) and 2,3-dimethylmalefic anhydride (DMMA) are conjugated to the amino groups of poly(ethylene glycol)-*b*-poly(L-lysine) (mPEG-*b*-PLL). The surface charge of the obtained mPEG-*b*-(PLL-*co*-(PLL-DMMA)-*co*-(PLL-DTPA-PTX)) nanoparticles (DMMA-NPs) can change from negative at blood pH to positive at tumor extracellular pH, implying that the DMMA-NPs will have a prolonged blood circulation time through avoiding rapid clearance by the reticuloendothelial system and an enhanced cell uptake at the tumor site. Compared to the control group, the *in vitro* studies show that the DMMA-NPs exhibit effective cellular uptake, rapid intracellular drug release, and significantly enhanced cytotoxicity against MCF-7 tumor cells, owing to the tumor-relevant pH and reductive conditions. These indicate that the charge-conversional DMMA-NPs provide an excellent platform for potential tumor therapy.

1 Introduction

In the last decade, polymeric drug delivery systems have emerged as a promising platform for cancer therapy.[1–6] Compared to the conventional chemotherapeutic agents, polymeric drug delivery systems for cancer therapy have the following advantages: (1) improving drug solubility; (2) altering the pharmacokinetics and tissue distribution; (3) prolonging circulation time through avoiding rapid clearance by the reticuloendothelial system; (4) enhancing the drug accumulation in the tumor tissue *via* the Enhanced Permeability and Retention (EPR) effect; (5) reducing the side effects.[7–9]

An effective nanoparticulate drug delivery system should possess multiple functions, such as a prolonged circulation time, enhanced cellular internalization, and rapid intracellular drug release. In recent years, stimuli-responsive drug-delivery systems have attracted great attention in cancer therapy. Typical biological stimuli include pH, temperature, redox and enzymes.[10–17] Among all of the stimuli, pH and redox are the two most attractive ones.[18] The pH value varies in normal tissues and tumor tissue, the normal physiological pH value in the blood and normal tissues is about 7.4, but the pH values in cancerous tissues (pH 6.5–7.2), endosomes and lysosomes (pH 4.5–6.5) are slightly acidic.[19,20] Thus pH-responsive nanoparticles can be designed to control drug release at a specific tumor site. For instance, Wang *et al.* reported a dual pH-sensitive polymer–drug conjugate nanoparticulate system for efficient anticancer drug delivery.[21] In addition, the concentration of glutathione (GSH) is different between the extracellular (~2.0 to 20.0 μM) and intracellular (~10 mM) environments, this redox-responsiveness can be used for rapid intracellular drug release.[17,22,23] For example, Zhang *et al.* reported a paclitaxel-loaded redox-sensitive micelles system which accomplished rapid drug release under reducing conditions.[24] Chen and co-workers reported redox and pH-responsive DOX-loaded micelles (PEG-SS-PTMBPEC), which showed a significant release of the protein at pH 6.0 or under reductive conditions containing 10 mM dithiothreitol (DTT) at pH 7.4 compared to that at normal physiological pH 7.4.[25]

Even though rapid progress has been made in the development of multi-stimuli-responsive nanoparticles, there are still some unresolved aspects that should be considered. Some nanoparticles were designed to achieve a high drug loading capacity and rapid intracellular drug release, but other aspects such as enhanced cellular internalization and prolonged circulation time, had not been considered.[26] In particular, a drug delivery system which can take advantage of the pH and redox

[a]*College of Chemistry, Northeast Normal University, Changchun 130024, P. R. China. E-mail: dengmx330@nenu.edu.cn*
[b]*Key Laboratory of Polymer Ecomaterials, Changchun Institute of Applied Chemistry, Chinese Academy of Sciences, Changchun 130022, P. R. China. E-mail: ztang@ciac.ac.cn*

dual responsiveness of carriers for prolonged blood circulation, enhanced cellular internalization and triggered intracellular release of payload, has seldom been reported.[27]

Therefore, in spite of the great efforts that have been made in the stimuli-responsive field, two intractable problems still remain. One is the contradiction between a long circulation time and the efficient tumor cellular uptake, as a prolonged circulation time needs a slightly negative charge on the polymeric surface while enhanced cellular internalization needs a positive charge on its surface. In the past few decades, persistent efforts have been made in charge-conversional nanoparticles. For example, Wang and co-workers designed zwitterionic polymer-based nanoparticles which exhibited a prolonged circulation time and promoted the tumoral cell internalization *in vivo*, owing to the charge switching.[28] The other problem is the contrasting requirement between the stability of nanoparticles during blood circulation and intracellular drug release. Cai and co-workers developed redox-responsive doxorubicin prodrug (DEX-PEI(-SS-DOX)) micelles which reduced drug leakage during blood circulation and improved the drug release rate through the stability of the drug conjugating and also, clearly the redox-responsive behavior.[29] Compared to drugs encapsulated through electrostatic or hydrophobic interactions, the drugs conjugated to nanocarriers through chemical bonds are relatively stable. So we decided to develop a polymer–drug conjugate which is stable in blood circulation and has a rapid drug release profile under intracellular conditions.

As previously described, we should solve all the problems in one system to achieve a high therapeutic efficiency. Therefore, a charge-conversional polymer–drug conjugate engineered with disulfide bonds was designed (Scheme 1). The conjugate is sensitive to both pH and redox stimuli. DTPA-PTX was conjugated to the amino groups of mPEG-*b*-PLL to produce the disulfide-contained polymer–PTX conjugate mPEG-*b*-(PLL-*co*-(PLL-DTPA-PTX)), where the disulfide bond would be cleaved under a high concentration of GSH (intracellular level), and thus the drug could be released rapidly in cells. The polymer–PTX conjugate was then modified with DMMA to produce mPEG-*b*-(PLL-*co*-(PLL-DMMA)-*co*-(PLL-DTPA-PTX)) nanoparticles (DMMA-NPs). DMMA was reacted with the amino group of the polymer–PTX conjugate, which generated a pH-sensitive amide bond and a carboxylic acid group. The amide bond remains stable at neutral and alkaline pH values, but is cleaved quickly under slightly acidic conditions. The nanoparticles should therefore ideally remain negatively charged at the blood pH, while change to positively charged at the tumor tissue pH. In addition, the

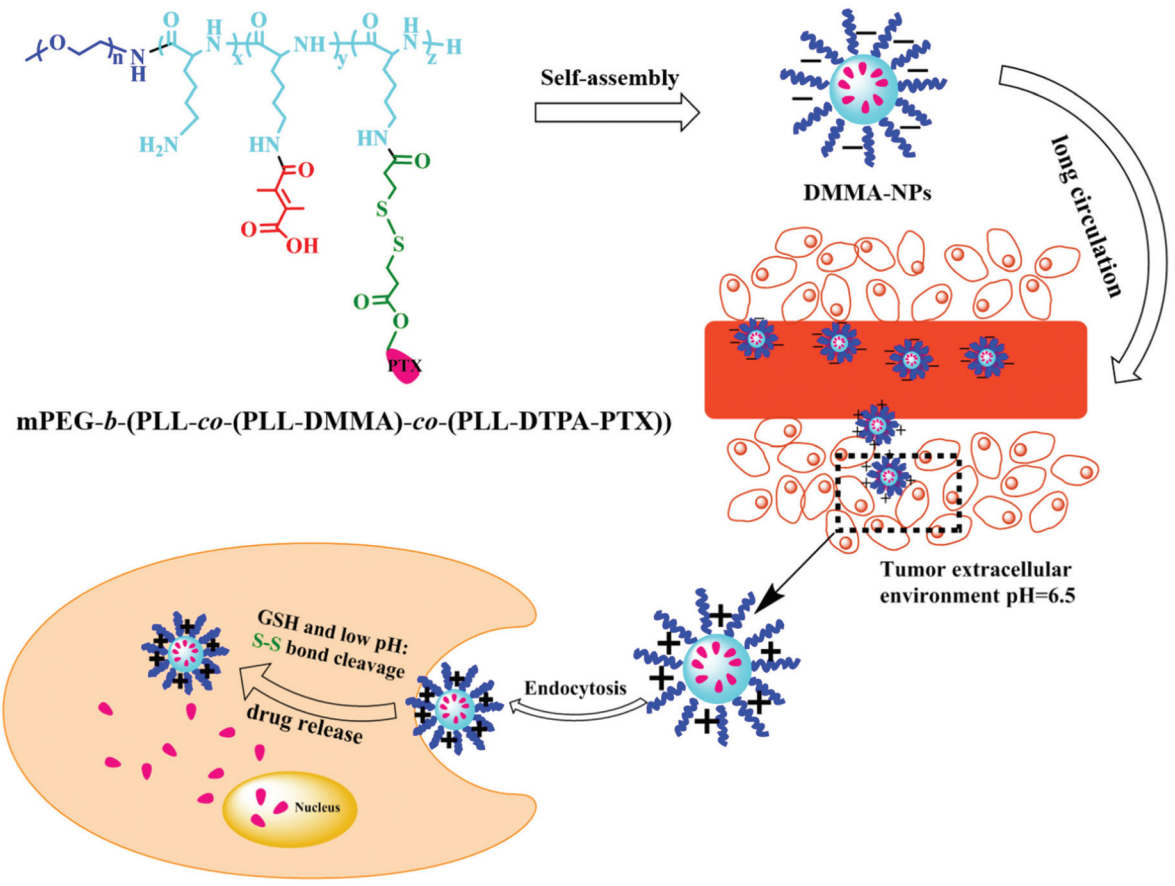

Scheme 1 Illustration of charge-conversional polymer–drug conjugate nanoparticles (DMMA-NPs) for a long circulation time, enhanced cellular uptake as well as intracellular redox-responsive release of PTX.

disulfide-contained nanoparticles have rapid intracellular drug release because of the reductive conditions in tumor cells.[30] Thus the drug delivery system has great potential to achieve the goals including a prolonged circulation time, enhanced cellular internalization and rapid intracellular drug release. In the present study, the preparation and characterization of DMMA-NPs as well as the *in vitro* tests were presented.

2 Experimental

2.1 Materials

Methoxyl poly(ethylene glycol) (mPEG, M_n = 5000) and 3,3′-dithiodipropionic acid (DTPA) were purchased from Aldrich and used as received. N^{ε}-Benzyloxycarbonyl-L-lysine (H-Lys(Z)-OH) was purchased from GL Biochem Co. Ltd (Shanghai, China). Amino-terminated methoxyl poly(ethylene glycol) (mPEG-NH_2, M_n = 5000) was prepared according to our previous work.[31] N^{ε}-Benzyloxycarbonyl-L-lysine-*N*-carboxyanhydride (Lys(Z)-NCA) was synthesized according to the literature.[32] *N*,*N*-Dimethylformamide (DMF) was stored over calcium hydride (CaH_2) and purified by vacuum distillation with CaH_2. Triethylamine (TEA) was dried and distilled with CaH_2. Paclitaxel (PTX) was purchased from Beijing Huafeng United Technology Company, China. 3-(4,5-Dimethyl-thiazol-2-yl)-2,5-diphenyl tetrazolium bromide (MTT) and 4′,6-diamidino-2-phenyl-indole dihydrochloride (DAPI) were purchased from Sigma and used as received. Fluorescein isothiocyanate (FITC), DMMA and glutathione (GSH) were purchased from Aladdin Reagent company, China. Succinic anhydride was purchased from Sinopharm Chemical Reagent Co. Ltd and used without further purification.

2.2 Synthesis of DTPA-PTX

In a 250 mL flame-dry flask, PTX (0.500 g, 0.585 mmol) was dissolved in 80 mL of dry THF. DTPA (0.185 g, 0.88 mmol) and EDC·HCl (0.340 g, 1.78 mmol) were then added and the mixture was stirred at 30 °C for 2 h. Subsequently, DMAP (0.073 g, 0.598 mmol) was added. The esterification reaction was maintained at 30 °C for 48 h. The solution was precipitated with 800 mL 0.1 M diluted hydrochloric acid. After filtration and drying under vacuum for 48 h, a white solid was obtained.

2.3 Synthesis of mPEG-*b*-PLL block copolymer

Methoxyl poly(ethylene glycol)-*b*-poly(L-lysine) (mPEG-*b*-PLL) was synthesized by the ring-opening polymerization of Lys-NCA using mPEG-NH_2 as a macroinitiator and by the subsequent deprotection of benzyloxycarbonyl groups. Typically, mPEG-NH_2 (3.00 g, 0.60 mmol) was dissolved in dry DMF (40 mL) after an azeotropic dehydration process with toluene. Then, Lys(Z)-NCA (3.43 g, 10.8 mmol) was dissolved in dry DMF (40 mL) and added to the mPEG-NH_2 solution in dry DMF *via* a syringe under nitrogen. The reaction mixture was stirred for 3 days at 30 °C under a dry nitrogen atmosphere and then precipitated into excess ice cold diethyl ether to obtain methoxy polyethylene glycol-*block*-poly-ε-(benzyloxycarbonyl)-L-lysine [mPEG-*b*-PLL(Z)].

mPEG-*b*-PLL was obtained through the deprotection of benzyloxycarbonyl groups on PEG-*b*-PLL(Z). In brief, mPEG-*b*-PLL(Z) (4.70 g) was dissolved in trifluoroacetic acid (47 mL). HBr/acetic acid (33 wt%) (6.15 mL) was then added at 0 °C. The reaction mixture was stirred for 45 min at 25 °C, and then precipitated into excessive ice cold diethyl ether. The product was further purified by dialyzed (MWCO 3500 Da) against distilled water. A white solid was obtained by lyophilization.

2.4 Synthesis of mPEG-*b*-(PLL-*co*-(PLL-DTPA-PTX))

3,3′-Dithiodipropionic acid modified PTX (DTPA-PTX) was conjugated to the amino groups of mPEG-*b*-PLL to obtain a disulfide-contained polymer–PTX conjugate mPEG-*b*-(PLL-*co*-(PLL-DTPA-PTX)). In brief, in a 50 mL flame-dry flask, DTPA-PTX (0.072 g, 0.069 mmol), EDC·HCl (0.039 g, 0.20 mmol) and NHS (0.024 g, 0.21 mmol) were dissolved in 10 mL of dry DMF and the reaction mixture was maintained under stirring for 12 h at room temperature. Subsequently, mPEG-*b*-PLL (0.50 g, 0.069 mmol) and TEA (0.015 g, 0.14 mmol) were dissolved in dry DMF, and then added into the above-mentioned solution drop by drop. The condensation reaction was maintained at 25 °C for 48 h. The solution was precipitated with an excess amount of ice cold diethyl ether. The product was dissolved in DMF and dialyzed (MWCO 3500 Da) against DMF to remove unreacted small molecules, then the solution was dialyzed (MWCO 3500 Da) against distilled water to remove the solvent DMF and the product was obtained by lyophilization.

2.5 Synthesis of mPEG-*b*-(PLL-*co*-(PLL-DMMA)-*co*-(PLL-DTPA-PTX))

The charge-conversional conjugate polymer mPEG-*b*-(PLL-*co*-(PLL-DMMA)-*co*-(PLL-DTPA-PTX)) (DMMA-NPs) was prepared as follows: mPEG-*b*-(PLL-*co*-(PLL-DTPA-PTX)) (0.10 g, 0.013 mmol) was dissolved in 20 mL of distilled water. The pH of the solution was adjusted to 8–9 by adding 0.1 M NaOH, and stirred for 2 h at room temperature. 2,3-Dimethylmalefic anhydride (DMMA) (0.475 g, 0.380 mmol) was then added, and in the process the pH of the solution was kept at 8–9 using 0.1 M NaOH. When the pH of the solution was constant, the reaction mixture was stirred for another 12 h. The solution was dialyzed (MWCO 3500 Da) against distilled water and a white solid was obtained by lyophilization.

As a control, mPEG-*b*-(PLL-*co*-(PLL-SA)-*co*-(PLL-DTPA-PTX)) (SA-NPs) was synthesized through a similar procedure as above. Details were described as follows: mPEG-*b*-(PLL-*co*-(PLL-DTPA-PTX)) (0.060 g, 0.0075 mmol) was dissolved in 15 mL of distilled water. The pH of the solution was adjusted to 8–9 by adding 0.1 M NaOH, and then stirred for 2 h at room temperature. Succinic anhydride (SA) (0.023 g, 0.23 mmol) was added several times to keep the pH ≈ 8–9 using 0.1 M NaOH. The subsequent steps were identical to the synthesis of mPEG-*b*-(PLL-*co*-(PLL-DMMA)-*co*-(PLL-DTPA-PTX)).

2.6 Synthesis of FITC-labeled NPs

mPEG-*b*-(PLL-*co*-(PLL-DTPA-PTX)) (50 mg) was dissolved in 2 mL of distilled water, and then FITC (2.5 mg) in DMF (3 mL) was added. After stirring for 24 h at room temperature in the dark, the solution was dialyzed (MWCO 3500 Da) against distilled water and then a yellow solid was obtained by lyophilization.

2.7 Characterization

^{1}H NMR, zeta potential, and dynamic laser scattering (DLS) were performed as in our previous studies.[33,34]

2.8 Calculation of the PTX loading content by elemental analysis

The drug loading content (DLC) of PTX in the DMMA-NPs was calculated according to equations:

$$\text{PTX wt\%} = (\text{mass of PTX in DMMA-NPs})/(\text{mass of DMMA-NPs}) \times 100\% \quad (1)$$

$$\text{PTX wt\%}/M(\text{PTX}) = \text{S wt\%}/2M(\text{S}) \quad (2)$$

where M(PTX) is the molecular weight of PTX, S wt% is the mass percent content of sulphur in the DMMA-NPs, M(S) is the atomic weight of sulphur.

2.9 Cell culture

Breast carcinoma MCF-7 cell lines were obtained from the Cell Bank of the Shanghai Institute of Biochemistry & Cell Biology in the Chinese Academy of Sciences and cultured at 37 °C under a 5% CO_2 atmosphere in Dulbecco's modified Eagle's medium (DMEM, Gibco) supplemented with 10% fetal bovine serum (FBS), penicillin (50 U mL^{-1}), and streptomycin (50 U mL^{-1}).

2.10 MTT assays

The cytotoxicities of DMMA-NPs and SA-NPs were evaluated against MCF-7 cells by the MTT assay.[35] MCF-7 cells were seeded in 96-well plates (6000 cells per well) in 100 μL of DMEM medium and incubated at 37 °C under a 5% CO_2 atmosphere for 24 h. The culture medium was replaced with 200 μL of fresh medium without fetal bovine serum (FBS) containing DMMA-NPs or SA-NPs at pH 7.4 or 6.5. After 3 h incubation, the medium was replaced with 200 μL of fresh medium at pH 7.4. After another 21 h or 45 h incubation, the cell viability was analyzed using MTT and

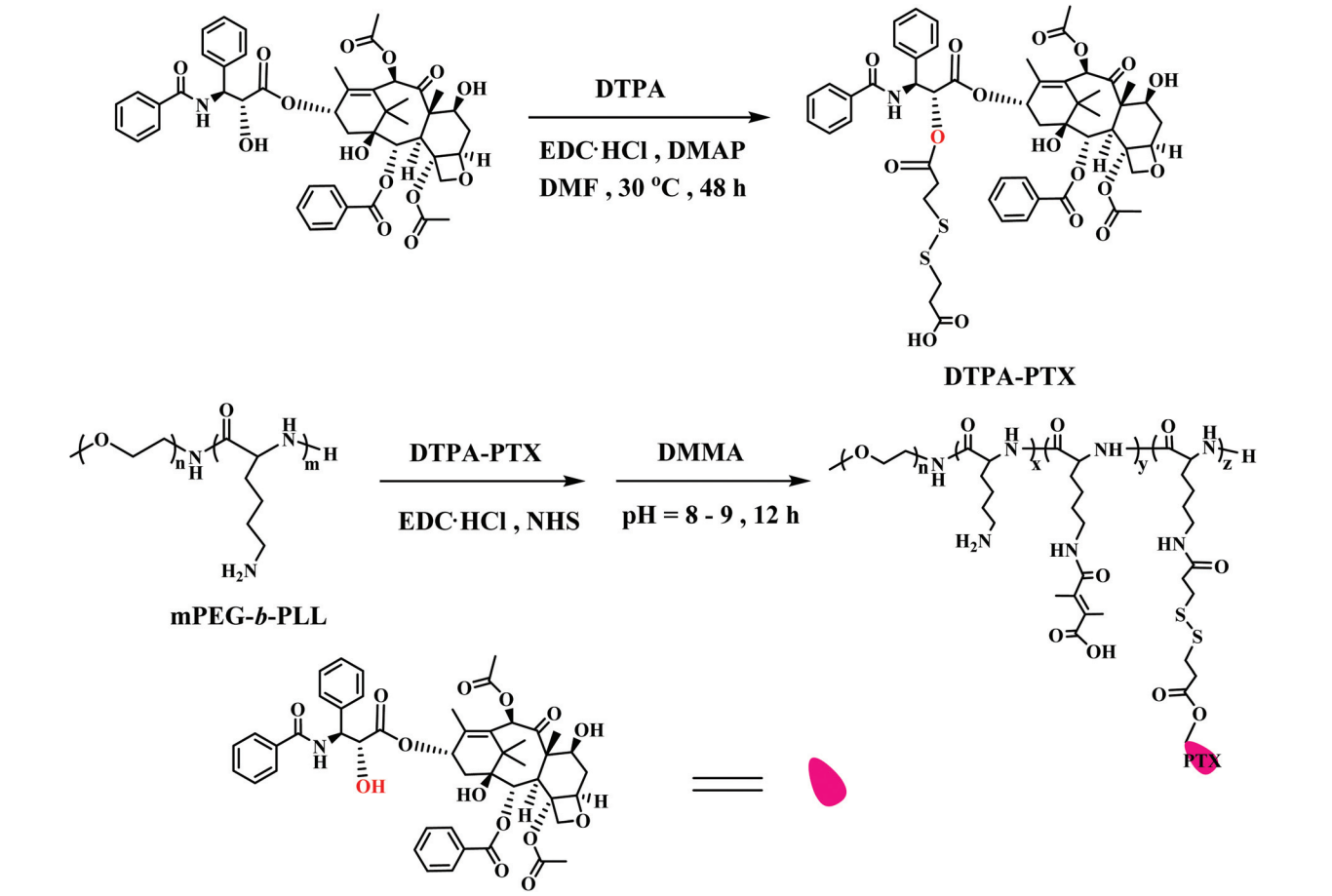

Scheme 2 Synthesis of mPEG-*b*-(PLL-*co*-(PLL-DMMA)-*co*-(PLL-DTPA-PTX)).

measured on a Bio-Rad 680 microplate reader at a wavelength of 490 nm.

2.11 Confocal laser scanning microscopy (CLSM) observation

MCF-7 cells were seeded in six-well plates at a density of 2 × 10^5 cells per well in 2 mL DMEM medium and incubated at 37 °C under a 5% CO_2 atmosphere for 24 h. The culture medium was replaced with 2 mL of fresh medium without FBS containing FITC-labeled DMMA-NPs or SA-NPs at pH 7.4 or 6.5. After 1 and 2 h of incubation, the cells were washed with PBS and fixed with 4% formaldehyde for 20 min at room temperature. The cell nuclei were stained by DAPI. Finally, the cells

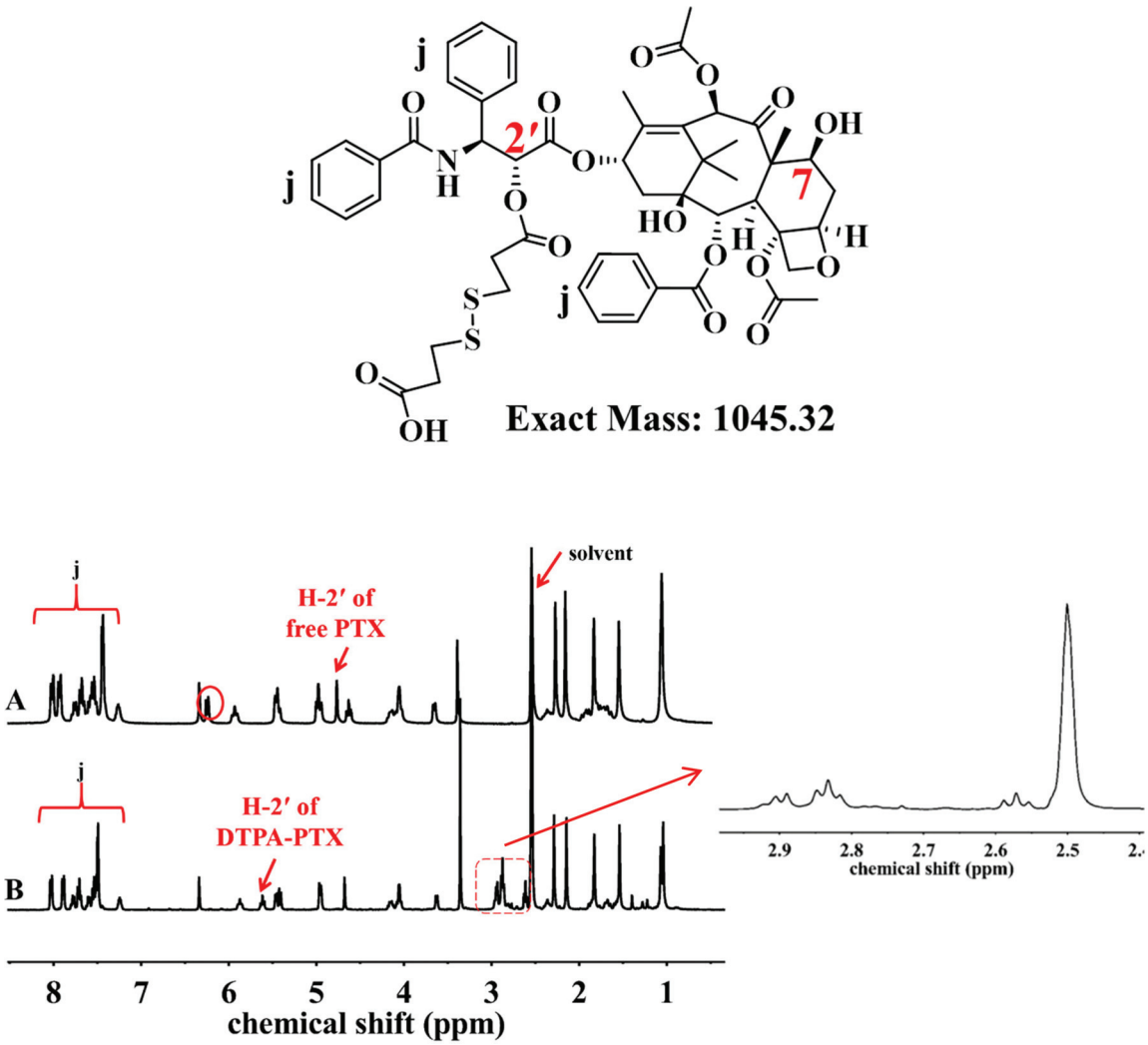

Fig. 1 ^{1}H NMR spectra of PTX (A) and DTPA-PTX (B) in DMSO-d_6.

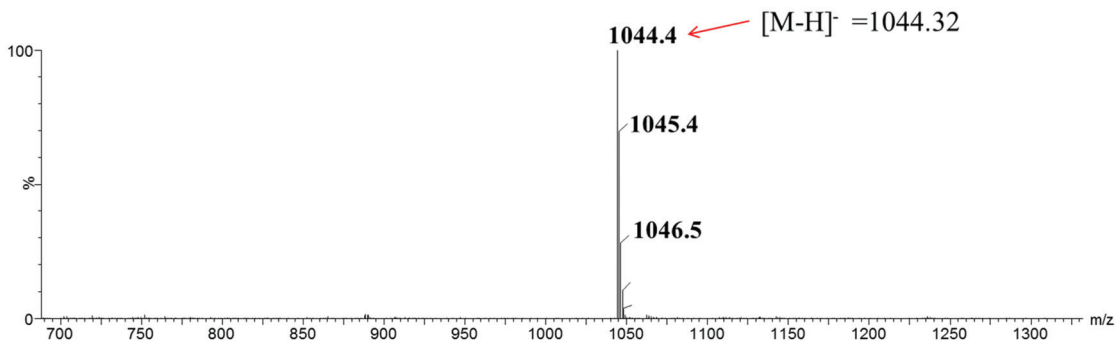

Fig. 2 ESI mass spectrum of DTPA-PTX.

were monitored by confocal laser scanning microscopy (Carl Zeiss LSM 780).

3 Results and discussion

3.1 Preparation and characterization of DMMA-NPs

The preparation of DMMA-NPs is shown in Scheme 2. First, DTPA-PTX and mPEG-*b*-PLL were synthesized; then, DTPA-PTX was conjugated to the amino groups of mPEG-*b*-PLL through condensation reaction, finally, DMMA or SA was conjugated to mPEG-*b*-(PLL-*co*-(PLL-DTPA-PTX)) through amide formation.

^{1}H NMR shows that DTPA was successfully conjugated to PTX, the signals at δ 2.87 ppm contributed to the methylene peaks of DTPA (–CH_2–C**H**$_2$–S–S–C**H**$_2$–CH_2–). Furthermore, through the comparison of the ^{1}H NMR spectra of free PTX and DTPA-PTX, the 2′-CH proton peak shifts from 4.76 ppm (free PTX) to 5.61 ppm (conjugated PTX). However, the 7-CH proton peak remains where it was before (Fig. 1). Therefore, the esterification reaction of PTX and DTPA took place preferentially at the 2′-hydroxyl of PTX instead of the 7-CH, as the 2′-hydroxyl of PTX has less steric hindrance than the 7-hydroxyl.[36,37] The ESI-MS of DTPA-PTX shows peaks at m/z = 1044.4 corresponding to the $(M - H)^-$, which is entirely consistent with the theoretical calculation value (Fig. 2).

In this study, mPEG-*b*-PLL was prepared as before. The ^{1}H NMR spectra of methoxyl poly(ethylene glycol)-*b*-poly(*N*$^\varepsilon$-benzyloxycarbonyl-L-lysine) [mPEG-*b*-P(LL(Z)] and mPEG-*b*-PLL (Fig. 3) confirmed that mPEG-*b*-PLL was synthesized successfully. All the peaks in the spectra were well assigned. The degree of polymerization (DP) of Lys(Z) units in mPEG-*b*-P(LL(Z)) was calculated by comparing the integration of methylene peaks of Lys(Z) groups (–CH_2–CH_2–CH_2–C**H**$_2$–NH) with the integration of methylene peaks of poly(ethylene glycol) (–C**H**$_2$–C**H**$_2$–O–). Finally, the DP of mPEG-*b*-P(LL(Z)) was calculated to be 17. Through a deprotection process of mPEG-*b*-P(LL(Z)), the typical peaks of carbobenzoxy groups at δ 5.13 and 7.25 ppm disappeared, indicating that the deprotection was complete. The DP of mPEG-*b*-PLL was also calculated to be 17 using the same method as for mPEG-*b*-P(LL(Z)).

Then, DTPA-PTX was conjugated to mPEG-*b*-PLL through a typical condensation reaction to obtain a disulfide containing polymer (mPEG-*b*-(PLL-*co*-(PLL-DTPA-PTX))). As shown in Fig. 4, comparing the ^{1}H NMR spectrum of mPEG-*b*-(PLL-*co*-(PLL-DTPA-PTX)) with that of DTPA-PTX, typical signals of the phenyl proton (7.2–8.0 ppm) of PTX appear, demonstrating that DTPA-PTX was successfully conjugated to mPEG-*b*-PLL. The DLC of PTX was calculated through two methods: one method was by comparing the peak integration of the phenyl proton of PTX with that of the PEG methylene proton signal (δ 3.5 ppm), the result was 10.3 wt% (Fig. 4); the other one was elemental analysis (EA), the DLC of PTX was calculated to be 7.9 wt% by analysis of the EA data (Table 1).

Finally, mPEG-*b*-(PLL-*co*-(PLL-DTPA-PTX)) was reacted with DMMA to obtain the charge-conversional nanoparticles DMMA-NPs. The characteristic resonance of the methyl

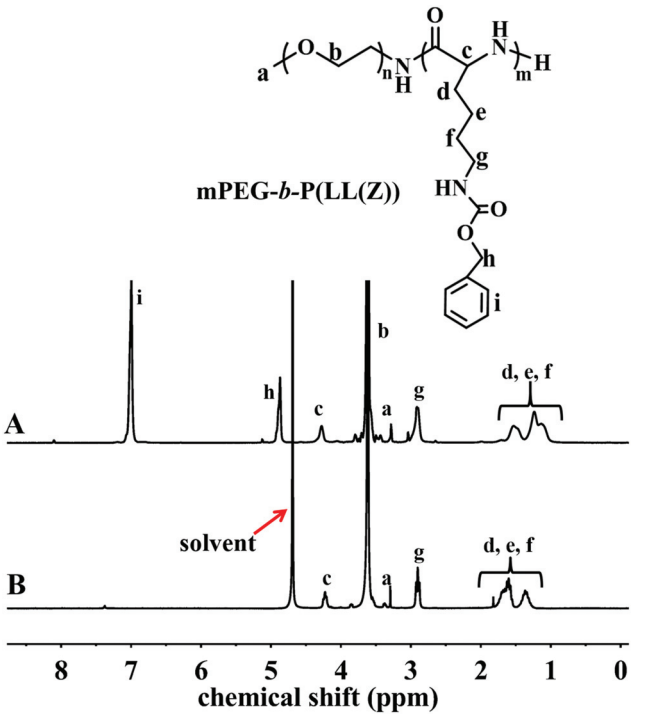

Fig. 3 ^{1}H NMR spectra of mPEG-*b*-P(LL(Z)) in CF_3COOD (A) and mPEG-*b*-PLL (B) in D_2O.

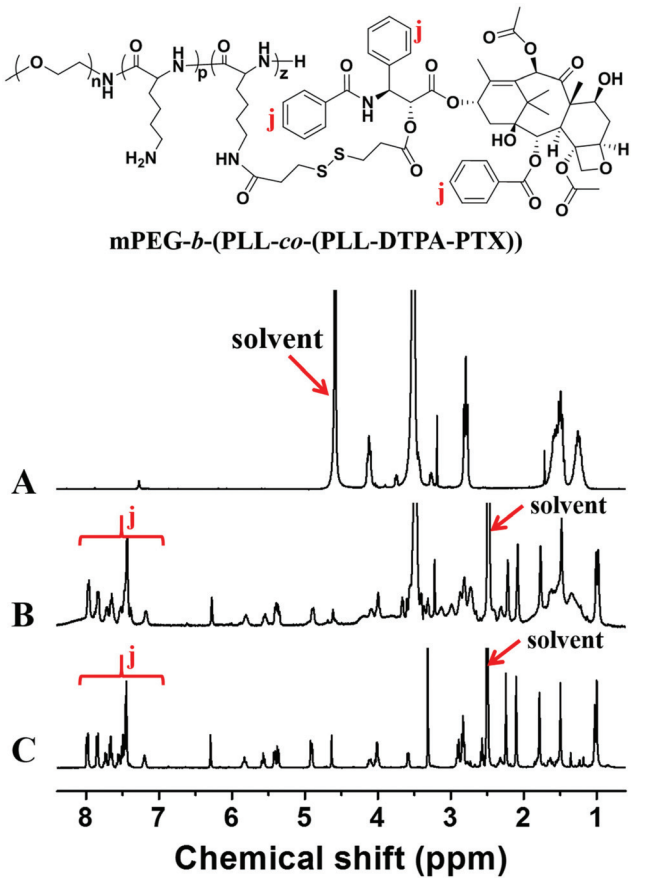

Fig. 4 ^{1}H NMR spectra of mPEG-*b*-PLL (A) in D_2O, mPEG-*b*-(PLL-*co*-(PLL-DTPA-PTX)) (B) and PTX (C) in DMSO-d_6.

Table 1 Elemental analysis of DMMA-NPs

	N (%)	C (%)	H (%)	S (%)
DMMA-NPs	3.79	50.12	7.251	0.596

(–C(C**H**$_3$)═C(C**H**$_3$)–) of DMMA at δ 1.64–1.87 ppm was displayed in the ^{1}H NMR spectrum of mPEG-*b*-(PLL-*co*-(PLL-DMMA)-*co*-(PLL-DTPA-PTX)), indicating that DMMA was successfully conjugated (Fig. 5). The degree of substitution of DMMA on PLL is 76%. mPEG-*b*-(PLL-*co*-(PLL-DTPA-PTX)) was reacted with succinic anhydride (SA) to obtain the non-charge reversal nanoparticles SA-NPs, where the degree of substitution of SA on PLL is 53%.

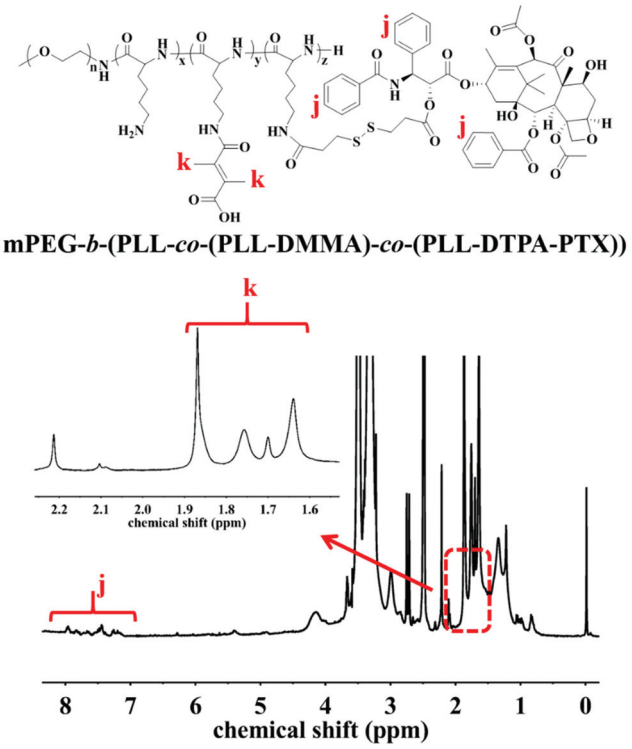

Fig. 5 ^{1}H NMR spectrum of mPEG-*b*-(PLL-*co*-(PLL-DMMA)-*co*-(PLL-DTPA-PTX)) in DMSO-d_6.

3.2 Dynamic laser scattering (DLS) and zeta potentials of DMMA-NPs

The sizes of nanoparticles in the sub-100 nm range are regarded as more effective for solid tumor penetration.[38,39] As shown in Fig. 6, the hydrodynamic radii (R_h) of DMMA-NPs and SA-NPs determined by DLS were 39.4 ± 10.9 and 35.7 ± 8.37 nm, respectively. This suggests that the nanoparticles should have a good penetration ability in solid tumors.

It is well known that cell membranes are negatively charged, so that the nanoparticles' surface charge plays an important role in cellular uptake. Neutral and slightly negatively charged nanoparticles have a prolonged circulation time as compared to positively charged nanoparticles, but they show poorer internalization as compared to the positively charged nanoparticles.[40] The DMMA-NPs have pH-sensitive DMMA groups that would be cleaved under slightly acidic conditions and resulted in the change of the zeta potential of nanoparticles. The zeta potentials of DMMA-NPs at pH 7.4 (blood pH) and pH 6.5 (tumor tissue pH) are shown in Fig. 7. The zeta potential of DMMA-NPs increased quickly at pH 6.5, it reached 0 mV in 6 min and became positive in 10 min. The zeta potential of DMMA-NPs at pH 7.4 also increased, but it increased at a much slower rate than that at pH 6.5. The increase in the zeta potential of DMMA-NPs stopped after 30 minutes at both pH 7.4 and pH 6.5. This indicated that the DMMA-NPs would be negatively charged in the normal physiological environment and have a long blood circulation time. After the DMMA-NPs reached tumor tissue sites, the slightly acidic pH would cause the break of the pH-sensitive DMMA amide bond and change the surface charge of the nanoparticles to positive, which would contribute to the internalization of the nanoparticles. In contrast, no significant increase of zeta potential was observed for SA-NPs, they maintained a negative charge around −22 mV at both pH 7.4 and pH 6.5. Therefore the SA-NPs were not charge-conversional nanoparticles and were quite different from the DMMA-NPs.

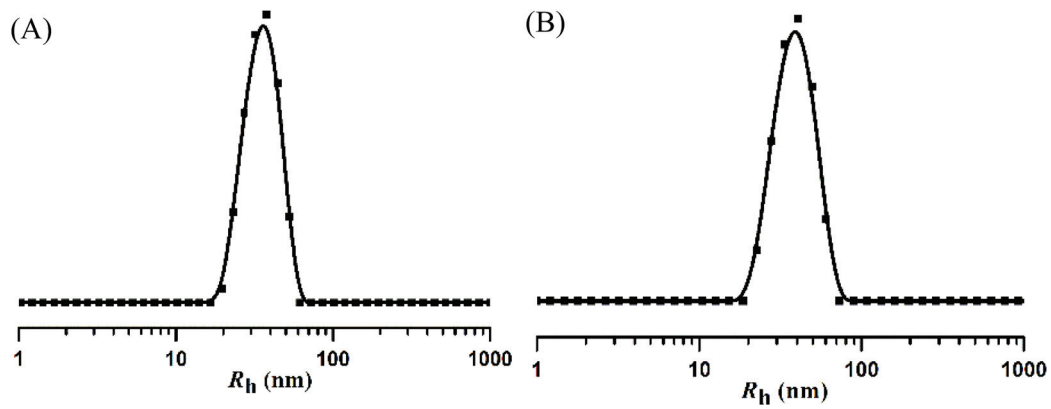

Fig. 6 Size of DMMA-NPs (A) and SA-NPs (B) determined by DLS.

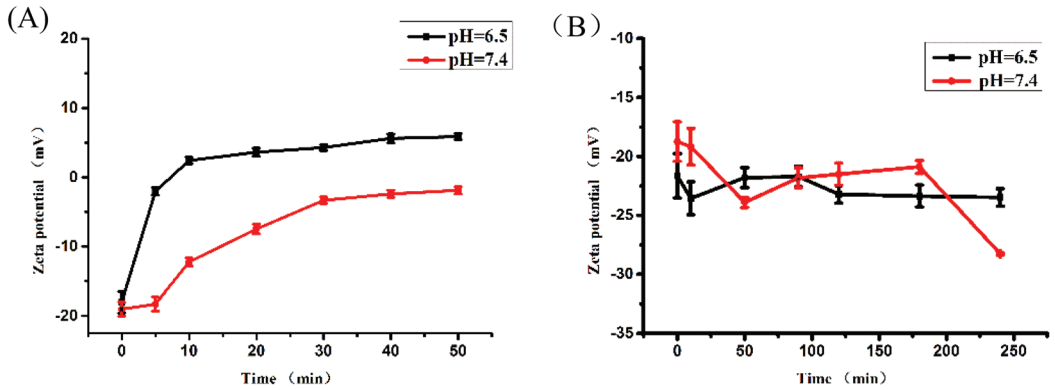

Fig. 7 Zeta potentials of DMMA-NPs (A) and SA-NPs (B) at pH = 6.5 and pH = 7.4 with different incubation times.

3.3 Cellular uptake of DMMA-NPs

Confocal laser scanning microscopy (CLSM) was used to investigate the cellular uptake behaviors of DMMA-NPs in MCF-7 breast carcinoma cancer cells at pH 7.4 and 6.5 (Fig. 8). DMMA-NPs were labeled by FITC for internalization investigation. After 1 h of incubation of DMMA-NPs at pH 6.5, some green fluorescence was observed in the cell membrane and

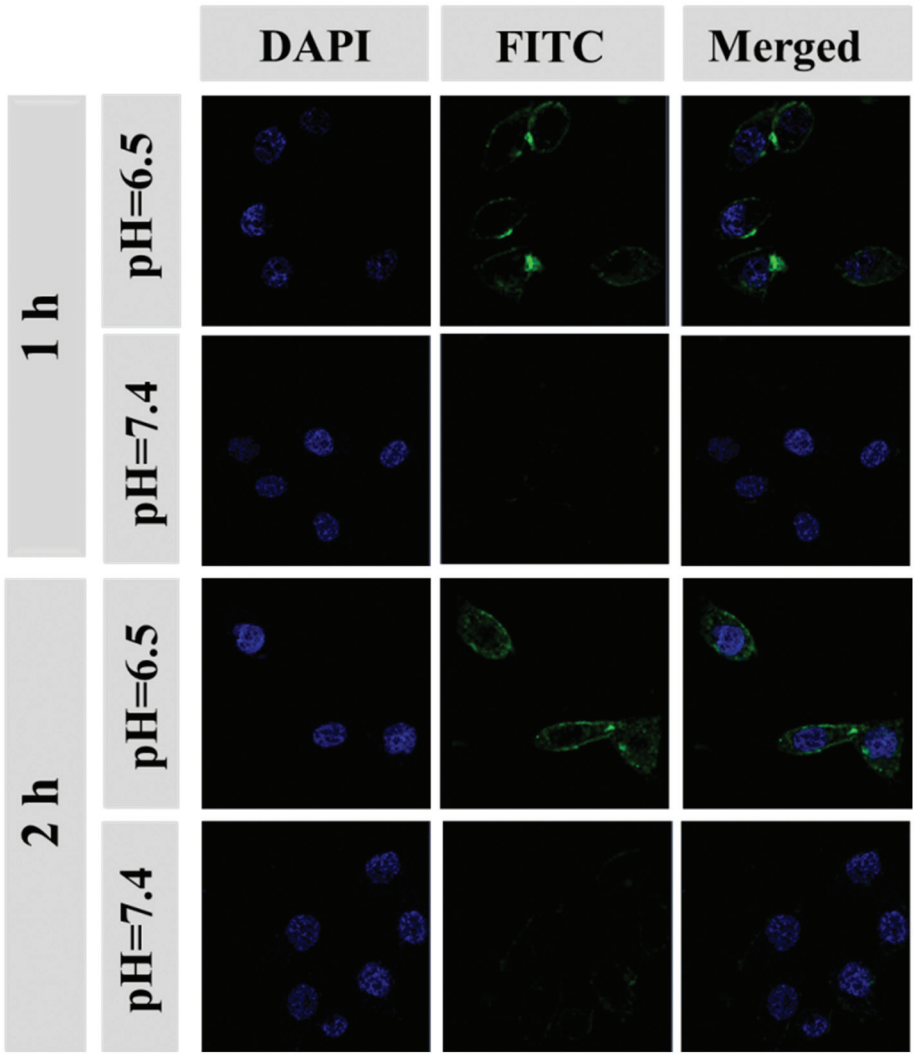

Fig. 8 Confocal laser scanning microscopy images of MCF-7 cells after incubation with FITC-labeled DMMA-NPs for 1 and 2 h at different pH.

cytoplasm, but little green fluorescence was observed at pH 7.4. After incubation for 2 h, the quantity of green fluorescence increased at both pH 7.4 and 6.5, the green fluorescence was distributed mostly in the cytoplasm at pH 6.5, but little green fluorescence was observed in the cell membrane at pH 7.4. Thus, the charge-conversional nanoparticles enhanced cell internalization significantly, which was consistent with the results of zeta potential analyses at pH 7.4 and 6.5.

3.4 *In vitro* cytotoxicity of copolymers

The *in vitro* cytotoxicities of charge-reversal DMMA-NPs and non-charge-reversal SA-NPs were evaluated using the MTT assay against the MCF-7 cell line in fresh serum-free DMEM at pH 7.4 and 6.5. As shown in Fig. 9, after incubation for 24 and 48 h, the cell viabilities of MCF-7 cells treated with DMMA-NPs were all about 80% at pH 7.4 even if the highest concentration reached 50 μg mL^{-1}. In contrast, the cell viabilities of MCF-7 cells incubated with DMMA-NPs could be less than 10% under the tumor extracellular pH 6.5, which indicated that the charge-reversal DMMA-NPs more effectively inhibited the proliferation of MCF-7 cells at pH 6.5 than at pH 7.4 (Fig. 9A and B). Compared to the charge-reversal DMMA-NPs, after incubation of 24 h and 48 h against MCF-7 cells, the cell viabilities of MCF-7 cells treated with non-charge-reversal SA-NPs were all above 70% at pH 7.4 and 6.5 (Fig. 9C and D) at all the incubation concentrations. These demonstrated that pH-sensitive charge-reversal DMMA-NPs exhibited a more effective inhibition proliferation against tumor cells at tumor extracellular pH_e 6.5 than non-charge-reversal SA-NPs. This phenomenon was also observed in Wang and co-workers' work on the NP/Pt@PPC-DA delivery system to overcome cisplatin resistance in cancer therapy.[41] In addition, owing to the existence of redox-responsive disulfide bonds in the nanoparticles, the charge-reversal DMMA-NPs at pH 7.4 and non-charge-reversal SA-NPs at pH 7.4 and 6.5 showed slight toxicity against MCF-7 tumor cells. This was demonstrated through *in vitro*

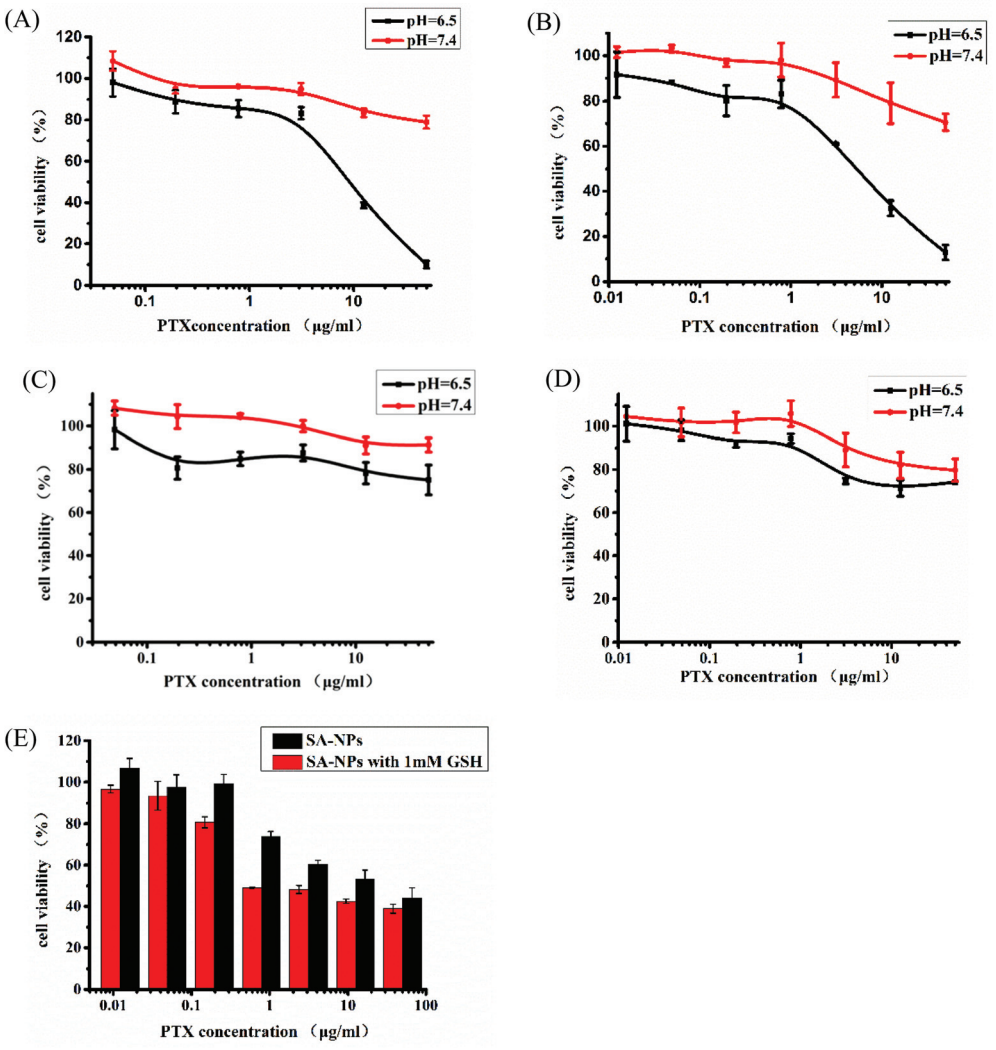

Fig. 9 *In vitro* cytotoxicity of DMMA-NPs at 24 h (A), 48 h (B); SA-NPs at 24 h (C), 48 h (D) to MCF-7 at different pH. *In vitro* cytotoxicity of SA-NPs incubated with free or 1 mM GSH to MCF-7 for 48 h (E).

cytotoxicity analyses of non-charge-reversal SA-NPs against the MCF-7 cell line in fresh DMEM at pH 7.4. MCF-7 cells were incubated for 1 h in fresh DMEM with 1 mM GSH or without, and then replaced with fresh DMEM containing non-charge-reversal SA-NPs for another 47 h. As shown in Fig. 9E, the half maximal inhibitory concentration (IC_{50}) of SA-NPs with non-GSH was 28 times higher than those treated with 1 mM GSH. This phenomenon contributed to the effect of disulfide linkages in the nanoparticles. A similar phenomenon was also observed in Chen and his co-workers' study on redox and pH-sensitive polymer–drug conjugates for the efficient delivery of paclitaxel.[30] In summary, the charge-conversional DMMA-NPs have an enhanced cellular uptake and inhibition against the proliferation of tumor cells.

4 Conclusions

In conclusion, we have successfully designed a pH and redox dual responsive polymer–drug conjugate for PTX delivery. The charge-reversal DMMA-NPs were well-synthesized through the conjugation of DTPA-PTX and DMMA to the amino groups of mPEG-*b*-PLL. The obtained DMMA-NPs' surface charge changed from negative at blood pH to positive at tumor extracellular pH. The charge reversal feature enhanced the cellular uptake of nanoparticles in the tumor extracellular environment. Subsequently the disulfide linkages in the nanoparticles were cleaved due to the intracellular redox reaction, leading to rapid drug release. Thus these demonstrate that the polymer–drug conjugate has advantages including a prolonged circulation time, enhanced cellular internalization and timely intracellular drug release, which enables the DMMA-NPs to be a promising alternative for tumor therapy.

Acknowledgements

This work is supported by the National Natural Science Foundation of China (Projects 51173184, 51233004, 51373168, 51390484, 51473029, 81430087 and 51403204), and the Program of Scientific Development of Jilin Province (20130206058GX and 20130521011JH).

References

1 Y. Matsumura and H. Maeda, *Cancer Res.*, 1986, **46**, 6387–6392.
2 Y. Bae and K. Kataoka, *Adv. Drug Delivery Rev.*, 2009, **61**, 768–784.
3 S. Kim, Y. Shi, J. Y. Kim, K. Park and J.-X. Cheng, *Expert Opin. Drug Delivery*, 2010, **7**, 49–62.
4 D. Peer, J. M. Karp, S. Hong, O. C. Farokhzad, R. Margalit and R. Langer, *Nat. Biotechnol.*, 2007, **2**, 751–760.
5 K. Kataoka, A. Harada and Y. Nagasaki, *Adv. Drug Delivery Rev.*, 2001, **47**, 113–131.
6 Y. Zhang, H. F. Chan and K. W. Leong, *Adv. Drug Delivery Rev.*, 2013, **65**, 104–120.
7 O. C. Farokhzad and R. Langer, *ACS Nano*, 2009, **3**, 16–20.
8 P. Burgess, P. B. Hutt, O. C. Farokhzad, R. Langer, S. Minick and S. Zale, *Nat. Biotechnol.*, 2010, **28**, 1267–1270.
9 N. Kamaly, Z. Xiao, P. M. Valencia, A. F. Radovic-Moreno and O. C. Farokhzad, *Chem. Soc. Rev.*, 2012, **41**, 2971–3010.
10 V. Torchilin, *Eur. J. Pharm. Biopharm.*, 2009, **71**, 431–444.
11 L. Stern, R. Perry, P. Ofek, A. Many, D. Shabat and R. Satchi-Fainaro, *Bioconjugate Chem.*, 2009, **20**, 500–510.
12 S. Ganta, H. Devalapally, A. Shahiwala and M. Amiji, *J. Controlled Release*, 2008, **126**, 187–204.
13 A. W. Alani, Y. Bae, D. A. Rao and G. S. Kwon, *Biomaterials*, 2010, **31**, 1765–1772.
14 Y. L. Li, L. Zhu, Z. Liu, R. Cheng, F. Meng, J. H. Cui, S. J. Ji and Z. Zhong, *Angew. Chem., Int. Ed.*, 2009, **48**, 9914–9918.
15 C. D. Austin, X. Wen, L. Gazzard, C. Nelson, R. H. Scheller and S. J. Scales, *Proc. Natl. Acad. Sci. U. S. A.*, 2005, **102**, 17987–17992.
16 N. Ma, Y. Li, H. Xu, Z. Wang and X. Zhang, *J. Am. Chem. Soc.*, 2009, **132**, 442–443.
17 F. Meng, W. E. Hennink and Z. Zhong, *Biomaterials*, 2009, **30**, 2180–2198.
18 N. Rapoport, *Prog. Polym. Sci.*, 2007, **32**, 962–990.
19 W. Chen, F. Meng, F. Li, S.-J. Ji and Z. Zhong, *Biomacromolecules*, 2009, **10**, 1727–1735.
20 J. Du, Y. Tang, A. L. Lewis and S. P. Armes, *J. Am. Chem. Soc.*, 2005, **127**, 17982–17983.
21 J.-Z. Du, X.-J. Du, C.-Q. Mao and J. Wang, *J. Am. Chem. Soc.*, 2011, **133**, 17560–17563.
22 G. Saito, J. A. Swanson and K.-D. Lee, *Adv. Drug Delivery Rev.*, 2003, **55**, 199–215.
23 R. Cheng, F. Feng, F. Meng, C. Deng, J. Feijen and Z. Zhong, *J. Controlled Release*, 2011, **152**, 2–12.
24 J. Li, M. Huo, J. Wang, J. Zhou, J. M. Mohammad, Y. Zhang, Q. Zhu, A. Y. Waddad and Q. Zhang, *Biomaterials*, 2012, **33**, 2310–2320.
25 W. Chen, P. Zhong, F. Meng, R. Cheng, C. Deng, J. Feijen and Z. Zhong, *J. Controlled Release*, 2013, **169**, 171–179.
26 L. Wu, Y. Zou, C. Deng, R. Cheng, F. Meng and Z. Zhong, *Biomaterials*, 2013, **34**, 5262–5272.
27 C. Yu, C. Gao, S. Lü, C. Chen, Y. Huang and M. Liu, *Chem. Eng. J.*, 2013, **228**, 290–299.
28 Y. Y. Yuan, C. Q. Mao, X. J. Du, J. Z. Du, F. Wang and J. Wang, *Adv. Mater.*, 2012, **24**, 5476–5480.
29 P. Liu, B. Shi, C. Yue, G. Gao, P. Li, H. Yi, M. Li, B. Wang, Y. Ma and L. Cai, *Polym. Chem.*, 2013, **4**, 5793–5799.
30 S. Lv, Z. Tang, D. Zhang, W. Song, M. Li, J. Lin, H. Liu and X. Chen, *J. Controlled Release*, 2014, **194**, 220–227.
31 H. Tian, C. Deng, H. Lin, J. Sun, M. Deng, X. Chen and X. Jing, *Biomaterials*, 2005, **26**, 4209–4217.
32 V. Dijk-Wolthuis, N. Wendelmoed, L. van de Water, P. van de Wetering, M. J. Van Steenbergen, J. J. Kettenes-van den Bosch, W. J. Schuyl and W. E. Hennink, *Macromol. Chem. Phys.*, 1997, **198**, 3893–3906.

33 H. Yu, Z. Tang, D. Zhang, W. Song, Y. Zhang, Y. Yang, Z. Ahmad and X. Chen, *J. Controlled Release*, 2015, **205**, 89–97.
34 W. Song, Z. Tang, D. Zhang, Y. Zhang, H. Yu, M. Li, S. Lv, H. Sun, M. Deng and X. Chen, *Biomaterials*, 2014, **35**, 3005–3014.
35 S. Lv, Z. Tang, M. Li, J. Lin, W. Song, H. Liu, Y. Huang, Y. Zhang and X. Chen, *Biomaterials*, 2014, **35**, 6118–6129.
36 Z. Xie, H. Guan, X. Chen, C. Lu, L. Chen, X. Hu, Q. Shi and X. Jing, *J. Controlled Release*, 2007, **117**, 210–216.
37 Y. Yu, C.-K. Chen, W.-C. Law, J. Mok, J. Zou, P. N. Prasad and C. Cheng, *Mol. Pharm.*, 2012, **10**, 867–874.
38 M. R. Dreher, W. Liu, C. R. Michelich, M. W. Dewhirst, F. Yuan and A. Chilkoti, *J. Natl. Cancer Inst.*, 2006, **98**, 335–344.
39 S. D. Perrault, C. Walkey, T. Jennings, H. C. Fischer and W. C. Chan, *Nano Lett.*, 2009, **9**, 1909–1915.
40 Y. Huang, Z. Tang, X. Zhang, H. Yu, H. Sun, X. Pang and X. Chen, *Biomacromolecules*, 2013, **14**, 2023–2032.
41 X.-Z. Yang, X.-J. Du, Y. Liu, Y.-H. Zhu, Y.-Z. Liu, Y.-P. Li and J. Wang, *Adv. Mater.*, 2014, **26**, 931–936.